Optical Materials 138 (2023) 113637

Contents lists available at ScienceDirect

Optical Materials

journal homepage: www.elsevier.com/locate/optmat

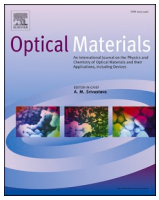

Research Article

Enhanced sunlight photo-catalytic performances of $ZnO/ZnNb_2O_6/Nb_2O_5$ composites for organic pollutant degradation

G. Essalah [a,*], H. Guermazi [a], S. Guermazi [a], J. Jedryka [b], K. Ozga [b], Albin Antony [c], A. Rao [d], P. Poornesh [d]

[a] Laboratory of Materials for Energy and Environment, and Modelling, Faculty of Science, University of Sfax, Soukra Road km 4 PB 1171, 3038, Sfax, Tunisia
[b] Chair of Automatic, Electrotechnical and Optoelectronics, Faculty of Electrical Engineering, Czestochowa University of Technology, Armii Krajowej 17, PL-42-201, Czestochowa, Poland
[c] Surface and Plasma Science, Charles University, Faculty of Mathematics and Physics, V Holešovičkách 2,180 00, Praha 8, Czech Republic
[d] Manipal Institute of Technology, Manipal Academy of Higher Education, Department of Physics, Manipal, 576104, Karnataka, India

ARTICLE INFO

Keywords:
$ZnO/ZnNb_2O_6/Nb_2O_5$
Linear optic
Nonlinear optic
Photocatalytic activity

ABSTRACT

The current study is focused on the development of zinc oxide-based ternary photo-catalysts that exhibit a good photocatalytic activity in methylene blue (MB) dye degradation, under sunlight irradiation. Indeed, the composites are prepared according to this proportion:(1-x) ZnO/xNb_2O_5, (x = 0; 0.01; 0.05; 0.1; 0.15; 0.2). In fact, X-ray diffraction patterns demonstrate that, for x = 0.01, a binary composite $ZnO/ZnNb_2O_6$ is formed. While ternary composite $ZnO/ZnNb_2O_6/Nb_2O_5$ is formed from x = 0.05. The linear and nonlinear optical properties are studied. So, compared to the ZnO (3.24 eV), the prepared composites exhibit a gap energy red-shift (3.18–3.22 eV), probably due to the interactions between oxide phases. Furthermore, the composites exhibit a high optical conductivity, which proves their high photo-responses. On the other hand, the increase of Nb_2O_5 amount led to an enhancement of nonlinear properties. Moreover, the photocatalytic tests demonstrate an excellent photocatalytic performance in MB degradation that reaches 100% after 120 min sun-light irradiation. Especially for 5% sample which exhibit also the best kinetic rate. These results allowed us to consider the $ZnO/ZnNb_2O_6/Nb_2O_5$ composites as promising materials for environmental applications.

1. Introduction

Currently, the filtration of polluted water through green photo-catalysis technology received increasing research interest due to its safe use, simple technology. And, more mainly its efficiency in the environmental protection against the probably contamination caused by industrial waste (textile, plastic, paper printing, leather applications …) [1,2]. The performance of photo-catalyst habitually depended on three agents: the irradiation range, the separation and the transfer of photo-generated charge carriers, and also of the mechanisms and the kinetic of surface reactions [3]. In fact, the band structure of photo-catalysts defined the adequate light irradiation. Where, most of the stable photo-catalysts had a wide bandgap, indicating a constricted light absorption range. Further, the photocatalytic process is given only by the photo-generated electrons and holes, which are transferred to the semiconductor surface. Whereas, most of them are immediately recombined in the massif phase of the catalysts [4]. In addition, the adsorption reaction of the dye at the surface of semiconductor must be established. For these reasons, we should be careful in the choice of catalyst material in order to institute the appropriate environment for photo-catalysis reaction. Consequently, elevated the dye degradation efficiency.

Indeed, zinc oxide (ZnO) presented a typical photosensitivity due to its appropriate characteristics such as wide band gap [5], high exciton binding energy (60 meV) [6], high intrinsic electron mobility (300 cm^2/Vs) [7] and especially high photo-catalytic activity [8]. Though, the photocatalytic efficiency can be limited by the fast electron–hole pair recombination [9]. To overcome this problem, we doped ZnO by other oxides such as the pentoxide niobium (Nb_2O_5), owing to its interesting properties serving to improve the photo-catalytic activity [10,11]. Among them we cited a strong redox ability and unique Lewis (LASs) and Brønsted acid sites (BASs) [12–14]. Beside, a greater reaction rate than those of others oxides [15]. Actually, the Nb_2O_5 presented an energy barrier, due to its large gap energy (3.3 eV), serving to reduce the

* Corresponding author.
E-mail address: essalahgmar2011@gmail.com (G. Essalah).

https://doi.org/10.1016/j.optmat.2023.113637
Received 4 November 2022; Received in revised form 18 January 2023; Accepted 26 February 2023
Available online 2 March 2023

Table 1
Description of the samples prepared by the solid-state technique.

x value	Samples notation	Composites
0	ZnO	
0.01	ZnNb1%	$ZnO/ZnNb_2O_6$
0.05	ZnNb5%	$ZnO/ZnNb_2O_6/Nb_2O_5$
0.1	ZnNb10%	$ZnO/ZnNb_2O_6/Nb_2O_5$
0.15	ZnNb15%	$ZnO/ZnNb_2O_6/Nb_2O_5$
0.2	ZnNb20%	$ZnO/ZnNb_2O_6/Nb_2O_5$

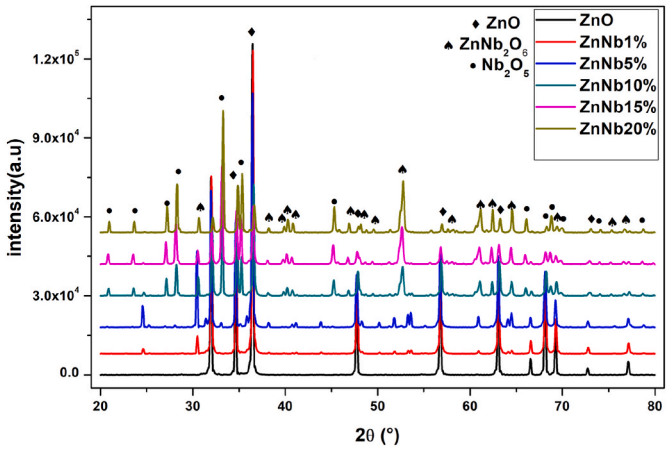

Fig. 1. XRD patterns of ZnO and $ZnO/ZnNb_2O_6/Nb_2O_5$ composites.

Table 2
The specific surface area and structural parameter values for the composites.

Sample	D_{cr} (nm)[a]	V (Å^3)	ρ (g cm^{-3})	SSA($g^{-1}m^2$)
ZnNb1%	14.98(9)	47.56 (5)	5.68 (2)	70.49 (1)
ZnNb5%	15.15(3)	47.89 (9)	5.64 (3)	70.17(4)
ZnNb10%	26.80(0)	47.31 (7)	5.71 (2)	39.18 (9)
ZnNb15%	9.37(4)	47.49 (3)	5.69 (1)	112.51(4)
ZnNb20%	45.46(0)	47.23 (5)	5.72 (2)	23.06(3)

[a] D_{cr} is calculated using Williamson-Hall model [20].

charge recombination. So, this oxide can be used as blocking layers avoiding electron back-transfer [16]. This fact is very essential for the photo-catalytic reaction success. The coupling between ZnO and Nb_2O_5 produced the formation of $ZnNb_2O_6$ phase, which presented a high photo-catalytic activity [17], due to its efficiency in the activation process of oxygen molecule (O_2) [18].

The challenge in this work is how to improve the catalyst's performance with the presence of three oxides in the same material: ZnO, $ZnNb_2O_6$, and Nb_2O_5. In this paper, we deploy the linear and the nonlinear properties of the composites. Optical parameters such as the band gap, the extinction coefficient, and the optical conductivity of the composites are computed. Then, the photocatalytic activities of our composites, for the degradation of the methylene blue dye, are investigated.

2. Experimental details

In this paper, all used materials (ZnO and Nb_2O_5) are supplied by Sigma Aldrich. For the elaboration of composites, we are used the solid-state method to mix together (1-x) ZnO/xNb_2O_5. The experimental details on the materials preparation are reported in our recent paper [19]. The description of the obtained powders is presented in Table 1.

The characterization of the prepared composites is carried out using diverse techniques. In fact, the linear optical properties are studied using the UV–visible PerkinElmer 365 spectrophotometry. Then, the nonlinear optical characterization is completed by measuring the second and third generated harmonics of the light (SHG and THG respectively). The photocatalytic activity of samples is studied via the degradation of methylene blue (MB) dye. These two recent characterizations are detailed in the following paragraphs.

2.1. Measurement of SHG and THG

To study the harmonics of the light (SHG or THG) generated by the tested materials, we achieved the following procedure. Source of fundamental radiation a 8 ns pulsed laser Nd:YAG with a wavelength at 1064 nm with frequency repetition 10 Hz is used. The power of the incident fundamental laser wavelength at 1064 nm is tuned by Glan's polarizer with laser damage power density 4 GW/cm^2. The laser beam profile diameter is equal to about 8 mm. The maximum of the energy is about 15,3 mJ for THG and 10,8 mJ for SHG. The value of fundamental laser energy signal is evaluated by the germanium photodetector and its second harmonic signal by a Hamamatsu photomultiplier with an installed interferometer filter at 532 nm or 355 nm with spectral width about 5 nm which transmits electromagnetic radiation with a wavelength at 532 nm or 355 nm. After passing through the diaphragm, the beam diameter is 2 mm. For the SHG study 50% signal amplification is applied. The studied samples are placed on a rotating table in a special cover. Levels of obtained fundamental and second harmonic signals are measured using a Tektronix MSO 3054 oscilloscope with sampling of 2.5 GS. The oscilloscope and the rotary table digit signals are inputted to the two channels of the oscilloscope connected with PC. The entire measuring stand is placed under the box eliminating the influence of external undesirable light scattering.

2.2. Photocatalytic test

The photocatalytic reaction is carried out in a photo-reactor using 50 ml of (MB) dye solution (10 mg/L) and 25 mg of catalysts. Firstly, the mixture is magnetically stirred for 30 min in dark, in order to guarantee the adsorption equilibrium between the couple catalyst/pollutant. Then, the solution is illuminated with sunlight at room temperature under continuous stirring. The total duration of photodegradation reaction is chosen equal to 120 min. Therefore, successive sampling is tacked each 15 min and the absorbance is measured by Shimadzu UV–vis spectrophotometer (model 1800UV–vis).

3. Results and discussions

3.1. Structural study

Structural investigation of the synthesized composites is carried out using XRD patterns (Fig. 1) [20]. The obtained results prove the formation of binary $ZnO/ZnNb_2O_6$ composite for the lower percent (1%), and the formation of ternary $ZnO/ZnNb_2O_6/Nb_2O_5$ composite for the highest percentages (5–20%) (Table 1). Furthermore, we notice that the average crystallite size increases in the composites compared to ZnO (Table 2). Besides, the specific surface area (SSA) can be estimated using the following relation Eq. (1) [21]:

$$SSA = \frac{6}{D_{cr} * \rho} \quad (1)$$

$$\text{where} \quad \rho = \frac{n * M}{N * V} \quad (2)$$

Where D_{cr} is the average crystallite size, ρ is the particle density [g m^{-3}], M is the molar mass of the substance M(ZnO) = 81.38 g mol^{-1}, n is the number of formula units in ZnO unit cell (n = 2) according to the JCPDS carte number: 96-210-7060, V is the unit cell volume, and N is Avogadro's number N = 6.02214.10^{23} mol^{-1}. SSA values for the composites are gathered in Table 2, it shows that the higher specific surface area is

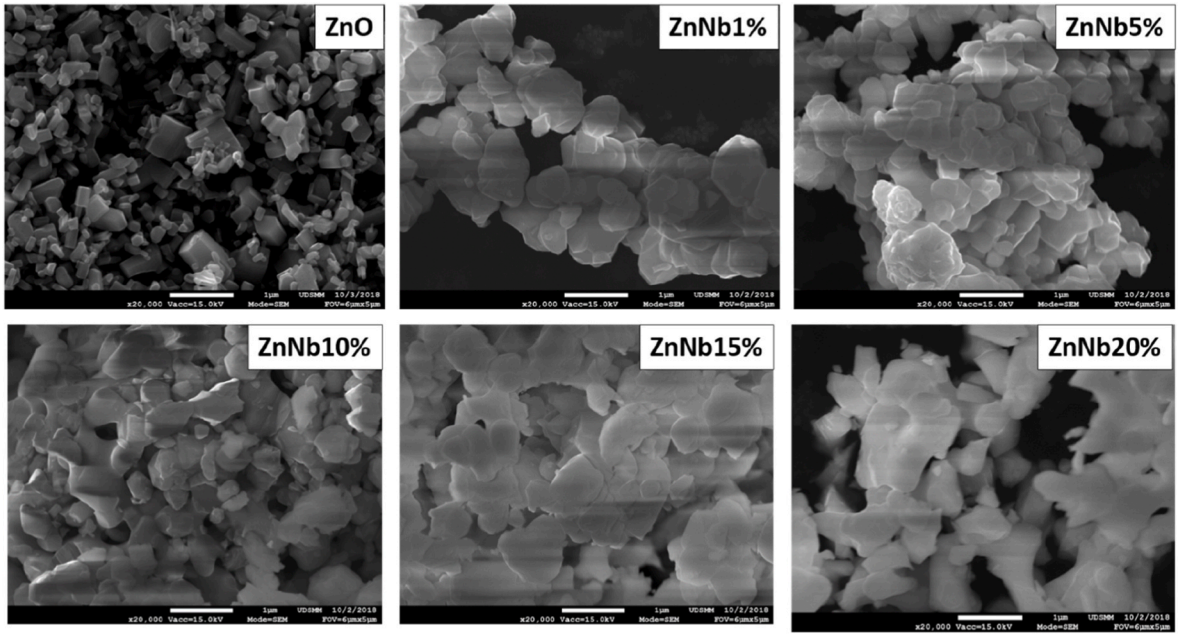

Fig. 2. SEM images of ZnO and ZnO/$ZnNb_2O_6$/Nb_2O_5 composites.

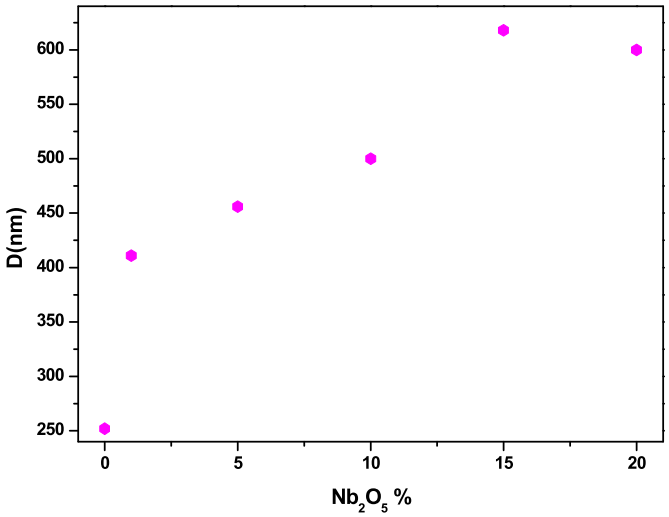

Fig. 3. The average grain size variation versus Nb_2O_5 content.

registered for the samples ZnNb1%, ZnNb5% and ZnNb15%. This result can predict that these samples may present the best photocatalytic activity, as this parameter has a great importance in the degradation process.

3.2. Morphological study

Fig. 2 shows the SEM images of all samples. In fact, the ZnO image demonstrates a heterogeneous grain size and shapes repartitions. On the other hand, composites images present more homogeneous grain repartition. Indeed, the variation of average grain size (Fig. 3) proves the increase of grain size with the increase of Nb_2O_5 content. It rises from 250 nm in ZnO to about 600 nm in composites with the highest percentage of Nb_2O_5 [20].

3.3. Linear optical study

Fig. 4 a displays the optical reflectance dispersion R(λ) for ZnO and composites, in the wavelength range 200–1100 nm. It is obvious that the binary ZnO/$ZnNb_2O_6$ composite (ZnNb1% sample) has the lowest reflectance (of about 80%) in the visible-near infrared region. While the

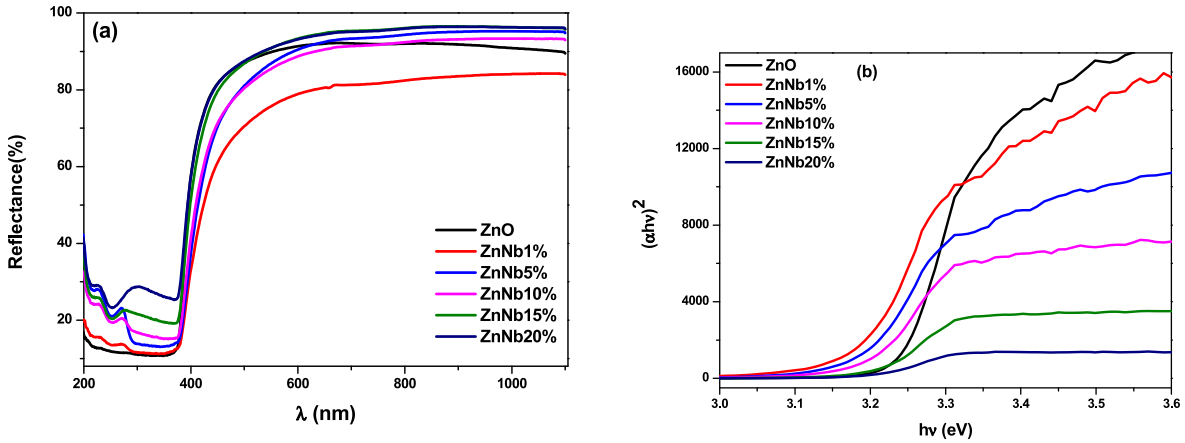

Fig. 4. a) Optical reflectance spectra of ZnO and composites, **b)** The tauc plots of ZnO and composites.

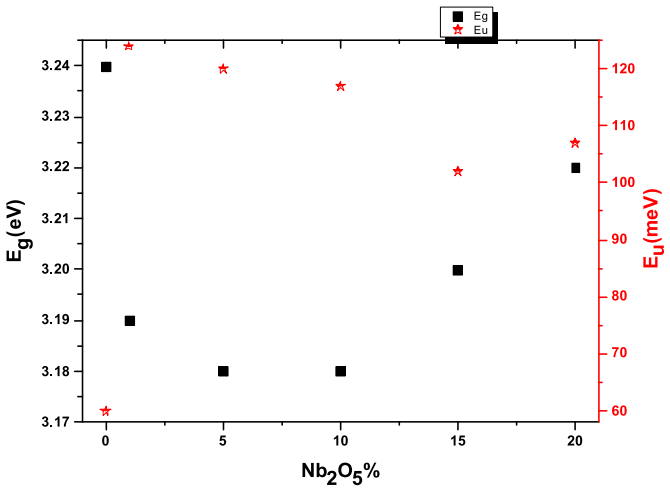

Fig. 5. The variation of gap and Urbach energy of ZnO and the composites.

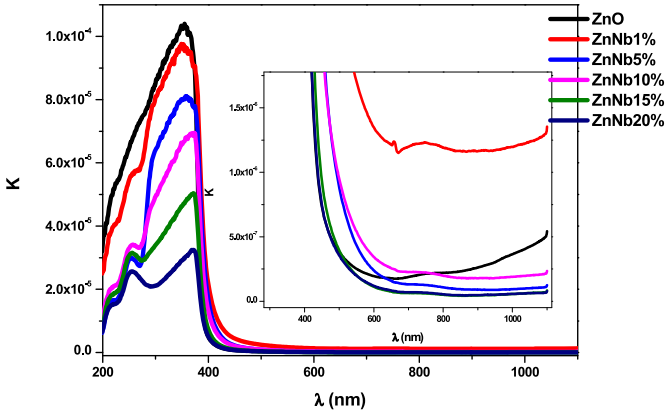

Fig. 6. The variation of the extinction coefficient for ZnO and the composites.

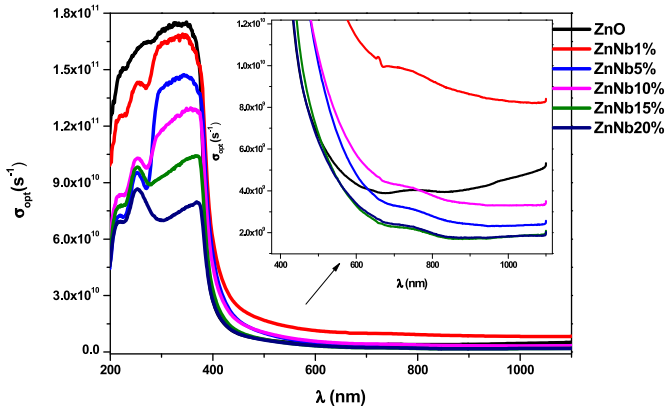

Fig. 7. Optical conductivity of ZnO and the composites.

reflectance reaches 90% in the ternary ZnO/$ZnNb_2O_6$/Nb_2O_5 composites. Moreover, the reflectance of composites increases in the UV-range as the Nb_2O_5 percent increases. Furthermore, it is observed that the reflectance edge shifts slightly towards the higher wavelength region (red shift) as the Nb_2O_5 percent increases, which could be related to the increase of grain size in the composites [22]. After that, we deduce the gap energy E_g values using Kubelka-Munk formula Eq. (3) [22,23], and by the mean of Tauc relation Eq. (4) [24,25]:

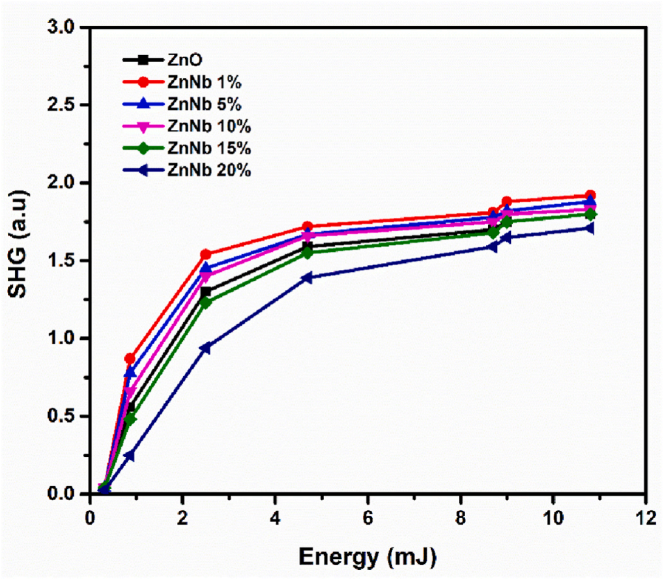

Fig. 8. The variation of the second generated harmonic as a function of energy for the composites.

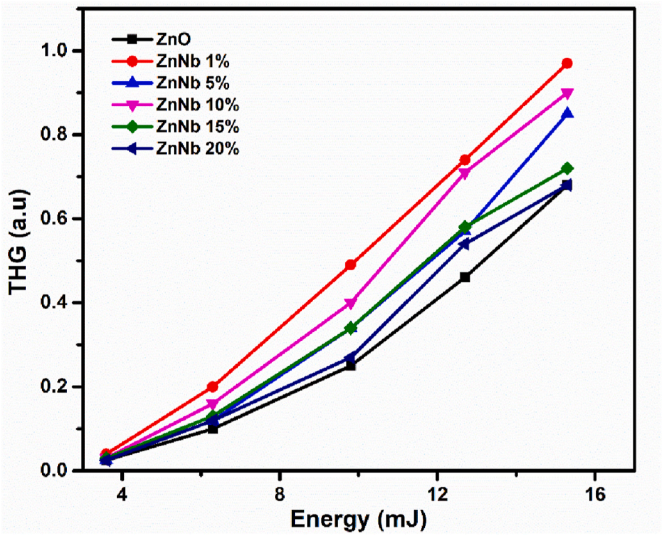

Fig. 9. The variation of the third generated harmonic as a function of energy for the composites.

$$F(R) = \frac{(1-R)^2}{2R} \tag{3}$$

$$\alpha h\vartheta = A\left(h\vartheta - E_g\right)^n \tag{4}$$

Where R is the sample's reflectance, A is a constant, hν is the photon energy and n is an exponent equal to 1/2 for a direct allowed transition, and $\alpha = \frac{F(R)}{t}$, t: is the pellet thickness.

In fact, by extrapolating the linear part of $(\alpha\, h\upsilon)^2$ vs. hυ plot (Fig. 4b), we determine the values of the optical band gap energy. For ZnO, we found E_g = 3.24 eV, then in the composites E_g exhibits a redshift (3.18–3.22 eV) (Fig. 5.). This red-shift is more important for the lower values of x (0.01; 0.05; and 0.1), then it decreases in the composites with higher content of Nb_2O_5. In fact, the gap energy is related with a charge transfer (electron) from the valence band (BV) to the conduction (BC), corresponding to the band-to-band transition [25,26]. Thus, the

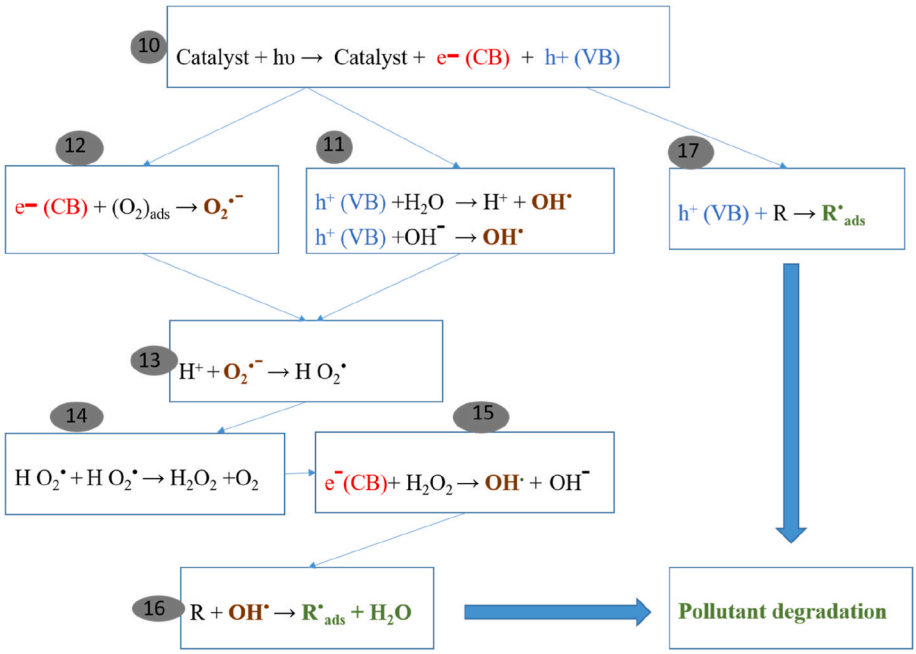

Scheme. 1. Photo-catalysis process.

reduction in the band gap energy of the composites, compared to ZnO, can be due to the enhancement of the charge transfer, between the two oxides phases in the ZnO/$ZnNb_2O_6$ composites, While the presence of Nb_2O_5 phase in the other composites reduce the charge transfer [27,28]. Similar results are reported by R. A. Rani et al. [21,29]. This fact can be due also to the increase in the concentration of defects in the material. Indeed, with the presence of defects, the electronic transition is made from the filled valence band to the energy levels of the defects instead to reaching the empty conduction band. In fact, doping is at the origin of the formation of localized states (band tail) leading to a reduction in the optical band gap [30,31]. This phenomenon, which causes the decrease in Eg, is usually in competition with another called Burstein-Moss effect, which induces, in contrary, the increase in the band gap after doping [32,33].

The incorporation of impurities in semiconductors induces often the formation of a tail band in the forbidden band. In this case, the inter-band optical transitions take place with an exponential dependence of the absorption coefficient α as a function of photon energy (hυ). Tape tail energy or Urbach energy E_U, associated with localized states due to defects, is calculated using Urbach's empirical law Eqs. (5) and (6) [34].

$$\alpha(h\vartheta) = \alpha_0 \exp\left(\frac{h\vartheta}{E_u}\right) \tag{5}$$

$$\frac{1}{E_u} = \frac{d(\ln(\alpha))}{d(h\vartheta)} \tag{6}$$

Fig. 5 shows that E_u increases in the composites compared to ZnO. This result confirms that the incorporation of Nb_2O_5 causes an increase in disorder and increases the concentration of defects in the composites. Then, with increasing Nb_2O_5 percent E_u decreases. It shows also an anti-proportionality between the variation of gap energy and that of Urbach one. This behavior proves that the optical gap of composites is basically directed by the disorder.

Moreover, the extinction coefficient (K) is very essential parameter to configure the optical applications. Where, the extinction coefficient is due to the absorption and light scattering [35], due to the interactions between electrons and photons in the material [36]. This parameter is expressed as a function of the absorption coefficient α and the incident wavelength λ by the following equation Eq. (7) [37]:

$$K = \frac{\alpha\lambda}{4\pi} \tag{7}$$

Fig. 6 shows that all the samples exhibit considerably low optical losses mainly in the visible and near infrared domains. Even in UV range, it has weak values, and decreases significantly with increasing Nb_2O_5 percent. This result proves that the composites have enhanced optical properties compared to ZnO, mainly in the UV.

Using the α and the refractive index (n) values we calculate the optical conductivity defined as bellow Eq. (8) [38]:

$$\sigma_{opt} = \frac{\alpha nc}{4\pi} \tag{8}$$

Where n is expressed by the following equation Eq. (9) [39]:

$$n = \sqrt{\frac{(1+R)^2}{(1-R)^2} - (K^2+1)} + \frac{1+R}{1-R} \tag{9}$$

Fig. 7 shows that, in the ultraviolet region, the ZnO has the higher optical conductivity values. Though even for the composites, the conductivity still prominent, and the higher value is recorded for ZnNb1%. After that, with Nb_2O_5 increasing, the conductivity decreases progressively. Whereas, in visible region, the ZnNb1% sample has the higher conductivity compared to ZnO and the other composites (inset of Fig. 7). The high conductivity of the elaborated samples proves that these composites have high photo-response nature, which suggests their suitability for optoelectronic device applications [40].

3.4. Nonlinear optical study

Figs. 8 and 9 shows the variation of ZnO's SHG and THG signals with the incorporation of Nb_2O_5. An increment in the signal intensity is observed for both SHG and THG signals with increasing Nb_2O_5 content. In SHG studies, samples with 1%, 5%, and 10% of Nb_2O_5 content shows higher signal intensity than ZnO. Whereas 15% and 20% samples result in the suppression of signal intensity. The observed enhancement in SHG signal intensity can be correlated with the structural effects induced in the composites. The XRD study shows that the addition of Nb_2O_5 creates defects in the materials [20]. The inclusion of defects in the compound

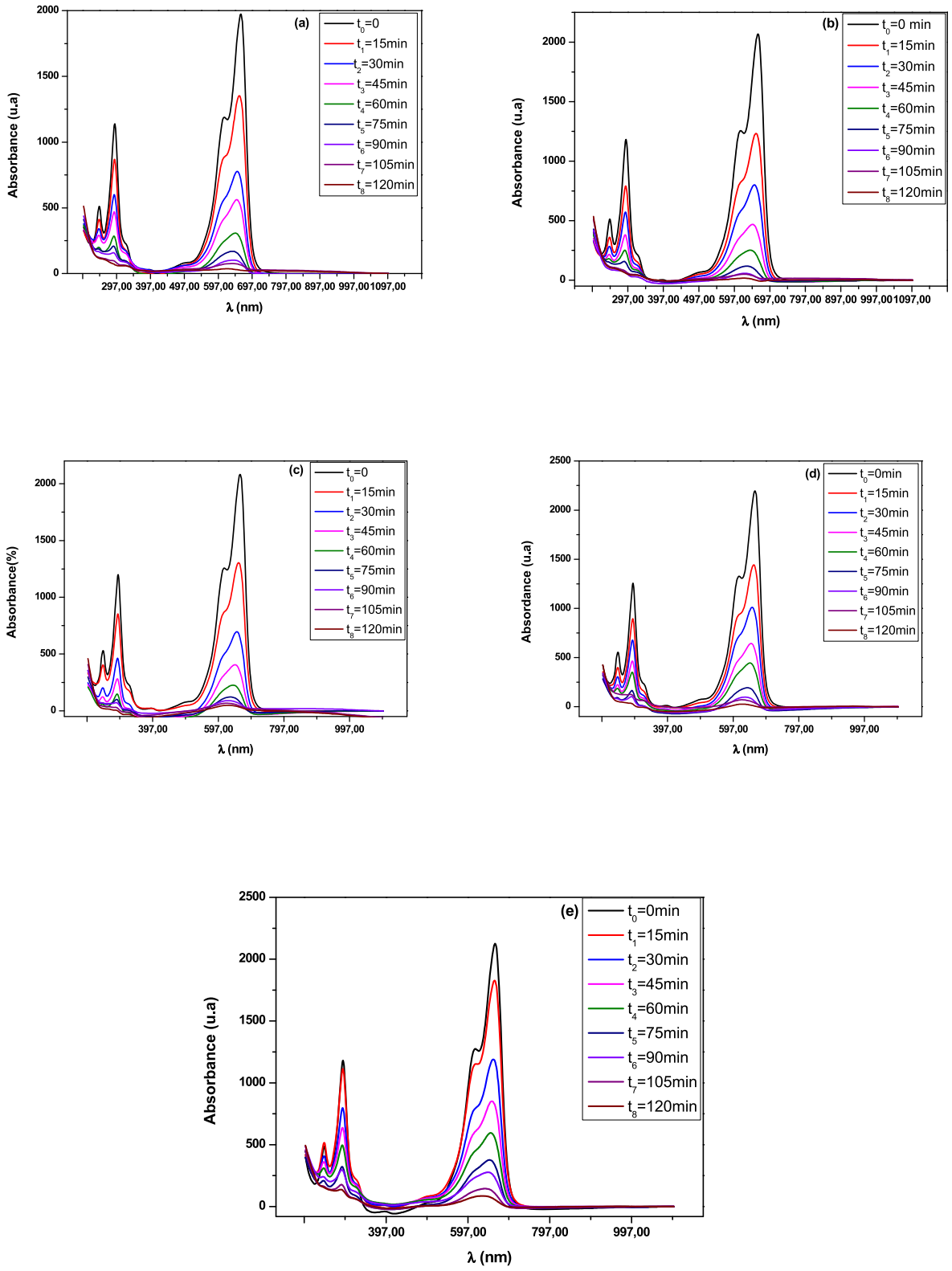

Fig. 10. The variation of MB absorption for the composites: (a) ZnNb1%, (b) ZnNb5%, (c) ZnNb10%, (d) ZnNb15%, (e) ZnNb20%.

results in the additional energy levels which results in the enhancement of SHG signal intensity [41]. A degradation of samples is observed for ZnNb15% and ZnNb20% when probed with fundamental beam which is a possible reason for the reduced signal intensity in these compounds.

The THG studies showed in Fig. 9 outcomes that all the composites show an enhancement in the signal intensity upon Nb_2O_5 incorporation. The origin of THG effects is different from SHG. Generally, THG effects raised in a material due to the change in the ground state dipole moments. In the present case, the observed enhancement in the THG intensity can be attributed to multiple mechanisms which change the dipole moment of the atoms [42]. The observed enhancement of THG efficiency in the composites can also be attributed to the defect states,

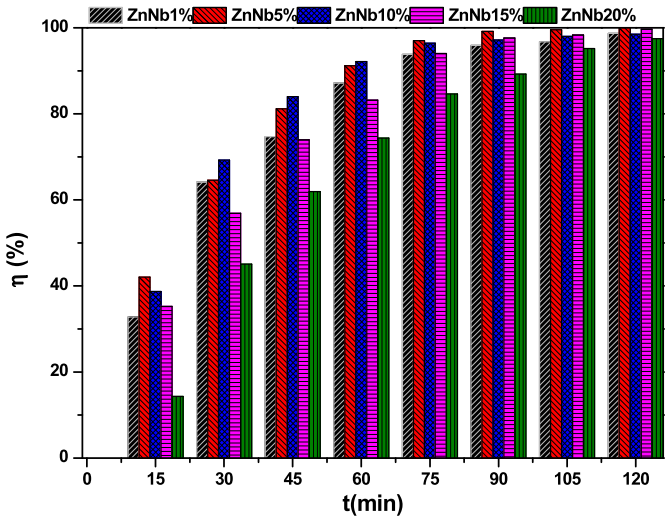

Fig. 11. The degradation efficiency of MB versus time for the composites.

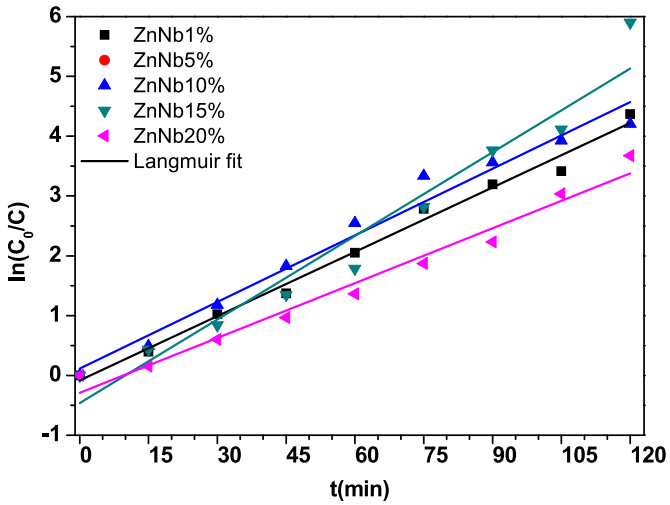

Fig. 12. Theoretical fit of MB photodegradation kinetics using the Langmuir model for the composites.

multiphoton process and occurrence of additional photo polarization which eventually changes the ground state dipole moments of the atoms [42]. Additionally, the laser stimulation further enhances THG signals due to laser-induced birefringence mechanism.

3.5. Photocatalytic activity

As the material is irradiated with sunlight having energy equal or higher than its band gap energy, an electron is promoted from the valence band (VB) to conduction band (CB), generating an electron/hole pair (e^-; in CB, h^+; in VB), Eq. (10). But this pair can be either recombined immediately (less than 1 ns) [43], or diffused to the surface of the semiconductor and perform redox reactions separately with other adsorbed elements like dyes molecules (R), water (H_2O), hydroxyl ions ($\boldsymbol{OH}^-$) and $\mathbf{O_2}$. In fact, the holes oxidize adsorbs H_2O or $\boldsymbol{OH}^-$ to produce hydroxyl radicals $\boldsymbol{OH}$ and $\mathbf{H}^+$ Eq. (11). Simultaneously, reactions between electrons and adsorbed dioxygen gives $\boldsymbol{O_2^-}$ Eq. (12). Then, extremely active hydroxyl radicals ($\boldsymbol{OH}$) are produced during successive reactions Eqs. (13-15). The ($\boldsymbol{OH}$) radicals degrade organic dyes R Eq. (16). In parallel, the reaction between holes and organic dyes can occur Eq. (17) [43,44]. The corresponding reactions of photo-degradation process are summarized in Scheme 1

Given the phase diversity in our composites (ZnO, Nb_2O_5, $ZnNb_2O_6$), this process is accelerated and then we obtain a suitable conditions for photo-catalysis reaction such us the enhancement in the production of $\boldsymbol{OH}$· and $\boldsymbol{O_2^-}$ radicals [45], and subsequently better degradation of the pollutant.

Fig. 10a-e. shows the dye absorption as a function of reaction time for the composites. It shows that the typical absorption peak of MB, positioned around 664 nm [46], is completely disappeared after 120 min of sunlight irradiation. So, the total degradation of the pollutant is clearly observed for all samples.

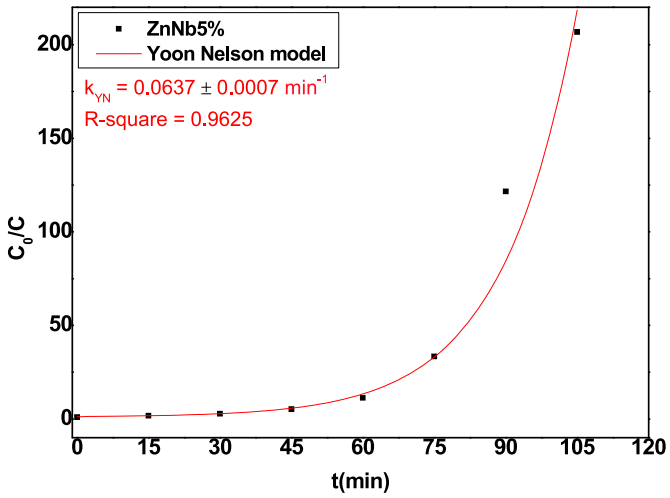

Fig. 13. Theoretical fit of MB photodegradation kinetics using the Yoon-Nelson model for ZnNb5% sample.

Table 4
The values of the kinetic rate constant k.

Samples	k_{LH} (min^{-1})	k_{YN} (min^{-1})
ZnNb1%	0.03586 ± 0.00132	–
ZnNb5%	–	0.0637 ± 0.0007
ZnNb10%	0.0371 ± 0.00215	–
ZnNb15%	0.04662 ± 0.00384	–
ZnNb20%	0.03056 ± 0.00179	–

Table 3
Recapitulative table of literature results and a comparison with our results.

Catalyst	Dye concentration (mgl^{-1})	Light source	Catalyst amount	Time(min)	Degradation%	Reference
Nb_2O_5/ZnO	20. phenol	sunlight	1 g/l	40	96	[22]
ZnO/$ZnNb_2O_6$	6.bromophenol	UV	20 mg	120	>80	[48]
Fe–Nb_2O_5	10. RhB	visible	100 mg	150	98	[49]
ZnO/Eu_2O_3/NiO	5. Methylene blue	sunlight	30 mg	150	98	[50]
TiO_2/ZnO/rGO	0.3. Methylene blue	Xe300W	0.1 g/l	120	92	[51]
Fe–ZnO	10. Methylene blue	UV	–	90	92	[52]
ZnO/$NiFe_2O_4$	50 Methylene blue	10W LED lamps	20 mg	40	92	[53]
ZnO/$ZnNb_2O_6$/Nb_2O_5	10 Methylene blue	sunlight	25 mg	90	100	this work

For further details about the photodegradation activity of our materials, we calculate the degradation efficiency η by the following equation Eq. (18) [47]:

$$\eta(\%) = \frac{C_0 - C}{C_0} * 100 \quad (18)$$

Where C_0 is the initial concentration of MB solution and C is the concentration at a given t.

Fig. 11 demonstrates that all composites exhibit an enhanced photodegradation efficiency and reaches 100% after 120 min. It is obviously noted that ZnNb5% shows the highest photodegradation activity. In fact, its MB photodegradation efficiency reaches 100% after only 90 min. Hence, the $ZnO/ZnNb_2O_6/Nb_2O_5$ composites exhibit enhanced photocatalytic efficiency compared to results reported in literature, as shown in Table 3.

Moreover, Fig. 11 shows that the MB photodegradation kinetic depends on the composite samples. Furthermore, to quantify the photodegradation kinetics of the MB; we fitted the experimental data to the Langmuir–Hinshelwood pseudo first order model [54]:

$$\ln\left(\frac{C_0}{C}\right) = k_{LH}t \quad (19)$$

Where k_{LH} is the first-order kinetic rate constant.

Fig. 12 confirms that the photocatalytic reaction follows the first-order kinetics according to the Langmuir–Hinshelwood model for all composites, except the ZnNb5%. For the later a second-order kinetics model, proposed by Yoon Nelson, is more suitable (Fig. 11) [55]:

$$\frac{C_0}{C} = 1 + \exp\left(-k_{YN}(t - \tau)\right) \quad (20)$$

Where k_{YN} is the Yoon–Nelson rate constant, τ is the necessary time to reach 50% of pollutant degradation, t is the time.

Fig. 13 shows the best fit to the experimental data for the ZnNb5% composite with the Yoon Nelson second-order kinetics model. The kinetic rate is found to be $k_{YN} = 0.0637 \pm 0.0007 min^{-1}$.

Table 4 shows the values of the rate constants for all catalysts. The high values of the kinetic constant prove the high degradation rate of all composites. These results confirm that the optimal photocatalytic degradation in $ZnO/ZnNb_2O_6/Nb_2O_5$ composites occurred when the Nb_2O_5 proportion is 5%. This fact proves that the presence of three phases (ZnO, $ZnNb_2O_6$, Nb_2O_5) in the material is an important factor for the success of photocatalytic process, as it expands the exchange surface with the pollutant and enhances the generation of actives radicals. In fact, the Nb_2O_5 phase serves as a blocking layer avoiding electron back-transfer by reducing the rapidity of the charge recombination [16,56]. While, the $ZnNb_2O_6$ phase activates the production process of oxygen molecules (O_2) [18]. Consequently, this leads to the enhancement of the kinetic and the efficiency of degradation reaction.

4. Conclusion

In this work, zinc oxide based ternary photo-catalysts is successfully prepared using solid state process. XRD analysis confirmed the formation of a $ZnO/ZnNb_2O_6$ binary composite for $x = 0.01$, and $ZnO/ZnNb_2O_6/Nb_2O_5$ ternary composite for the higher adding proportion. Optical investigation results showed that the composites exhibit a red-shift of the gap energy (3.18–3.22 eV), compared to the ZnO (3.24 eV), due to the interactions between oxide phases. Furthermore, we demonstrated that all composites exhibited an enhanced photodegradation efficiency of MB dye degradation under sun-light irradiation, that reached 100% after 120 min. Obviously, ZnNb5% has the highest MB photodegradation efficiency which reached 100% after only 90 min. This particular photocatalytic activity of this composite is explained by the faster kinetic MB degradation reaction compared to the other composites. In fact, the photocatalytic reaction followed the L–H first-order kinetics model for all composites, except the ZnNb5% for which a Y–N second-order kinetics model is more suitable. These results allowed us to consider the $ZnO/ZnNb_2O_6/Nb_2O_5$ composites as promising materials for environmental applications such as waste-water remediation.

Funding

This research was supported by the Tunisian Ministry of High Education and Scientific Research.

CRediT authorship contribution statement

G. Essalah: Roles/. **H. Guermazi:** Supervision, Writing – review & editing, Validation, Investigation, Project administration. **S. Guermazi:** Resources, Funding acquisition, Project administration. **J. Jedryka:** Data curation, Methodology. **K. Ozga:** Data curation, Methodology. **Albin Antony:** Data curation, Methodology. **A. Rao:** Methodology, Software, Investigation. **P. Poornesh:** Methodology, Software, Investigation.

Declaration of competing interest

The authors declare that they have no known competing financial interests or personal relationships that could have appeared to influence the work reported in this paper.

Data availability

Data will be made available on request.

Acknowledgements

Authors gratefully thank the financial support of the Tunisian Ministry of higher education and scientific research.

References

[1] M. Fang, X. Tan, Z. Liu, B. Hu, X. Wang, Recent progress on metal-enhanced photocatalysis: a review on the mechanism, Research 2021 (2021), https://doi.org/10.34133/2021/9794329.
[2] N.A.F. Al-Rawashdeh, O. Allabadi, M.T. Aljarrah, Photocatalytic activity of graphene oxide/zinc oxide nanocomposites with embedded metal nanoparticles for the degradation of organic dyes, ACS Omega 5 (2020) 28046–28055, https://doi.org/10.1021/acsomega.0c03608.
[3] Y. Zhang, X. Liu, M. Yusoff, M.H. Razali, Photocatalytic and antibacterial properties of a 3D flower-like TiO2 nanostructure photocatalyst, Scanning 2021 (2021), e3839235, https://doi.org/10.1155/2021/3839235.
[4] Y.-J. Xu, Promises and challenges in photocatalysis, Front. Catal. (2021), https://doi.org/10.3389/fctls.2021.708319, 0.
[5] J.E. Morales-Mendoza, F. Paraguay-Delgado, J.A.D. Moller, G. Herrera-Pérez, N. Pariona, Structure and optical properties of ZnO and ZnO2 nanoparticles, J. Nano Res. 56 (2019) 49–62. https://doi.org/10.4028/www.scientific.net/JNanoR.56.49.
[6] S. Kumar, K. Asokan, R.Kr Singh, S. Chatterjee, D. Kanjilal, A.K. Ghosh, Structural and optical properties of ZnO and ZnO:Fe nanoparticles under dense electronic excitations, J. Appl. Phys. 114 (2013), 164321, https://doi.org/10.1063/1.4826525.
[7] Y. Chimupala, C. Phromma, S. Yimklan, N. Semakul, P. Ruankham, Dye wastewater treatment enabled by piezo-enhanced photocatalysis of single-component ZnO nanoparticles, RSC Adv. 10 (2020) 28567–28575, https://doi.org/10.1039/D0RA04746E.
[8] A.A. Yaqoob, N.H. binti M. Noor, K. Umar, R. Adnan, M.N.M. Ibrahim, M. Rashid, Graphene oxide–ZnO nanocomposite: an efficient visible light photocatalyst for degradation of rhodamine B, Appl. Nanosci. 11 (2021) 1291–1302, https://doi.org/10.1007/s13204-020-01665-8.
[9] H. Wang, L. Zhang, Z. Chen, J. Hu, S. Li, Z. Wang, J. Liu, X. Wang, ChemInform abstract: semiconductor heterojunction photocatalysts: design, construction, and photocatalytic performances, Chem. Soc. Rev. (2014), https://doi.org/10.1039/c4cs00126e.
[10] G. Carvalho, M. Siqueira, M. Nascimento, M. Oliveira, G. Amarante, Nb2O5 supported in mixed oxides catalyzed mineralization process of methylene blue, Heliyon 6 (2020), e04128, https://doi.org/10.1016/j.heliyon.2020.e04128.

[11] H. Liu, N. Gao, M. Liao, X. Fang, Hexagonal-like Nb2O5 nanoplates-based photodetectors and photocatalyst with high performances, Sci. Rep. 5 (2015) 1–9, https://doi.org/10.1038/srep07716.
[12] Y. Zhao, X. Zhou, L. Ye, S.C.E. Tsang, Nanostructured Nb2O5 catalysts, Nano Rev. 3 (2012), 17631, https://doi.org/10.3402/nano.v3i0.17631.
[13] I. Nowak, M. Ziolek, Niobium compounds: preparation, characterization, and application in heterogeneous catalysis, Chem. Rev. 99 (1999) 3603–3624, https://doi.org/10.1021/cr9800208.
[14] B.T. da Fonseca, E. D'Elia, J.M. Siqueira Júnior, S.M. de Oliveira, K.L. dos Santos Castro, E.S. Ribeiro, Study of the characteristics and properties of the SiO2/TiO2/Nb2O5 material obtained by the sol–gel process, Sci. Rep. 11 (2021) 1–15, https://doi.org/10.1038/s41598-020-80310-4.
[15] K. Su, H. Liu, Z. Gao, P. Fornasiero, F. Wang, Nb2O5-Based photocatalysts, Adv. Sci. 8 (2021), https://doi.org/10.1002/advs.202003156.
[16] T. Valerio, G. Maia, L. Gonçalves, A. Viomar, E. Banczek, P. Rodrigues, Study of the Nb2O5 insertion in ZnO to dye-sensitized solar cells, Mater. Res. 22 (2019), https://doi.org/10.1590/1980-5373-mr-2018-0864.
[17] A. Kormányos, A. Thomas, M.N. Huda, P. Sarker, J.P. Liu, N. Poudyal, C. Janáky, K. Rajeshwar, Solution combustion synthesis, characterization, and photoelectrochemistry of CuNb2O6 and ZnNb2O6 nanoparticles, J. Phys. Chem. C 120 (2016) 16024–16034, https://doi.org/10.1021/acs.jpcc.5b12738.
[18] J. Wang, X. Gu, L. Pei, P. Kong, J. Zhang, X. Wang, R. Wang, E.R. Waclawik, Z. Zheng, Strong metal-support interaction induced O2 activation over Au/MNb2O6 (M = Zn2+, Ni2+ and Co2+) for efficient photocatalytic benzyl alcohol oxidative esterification, Appl. Catal. B Environ. 283 (2021), 119618, https://doi.org/10.1016/j.apcatb.2020.119618.
[19] G. Essalah, G. Leroy, J.C. Carru, B. Duponchel, M. Mascot, C. Poupin, R. Cousin, S. Guermazi, H. Guermazi, Conduction mechanisms and relaxation phenomena along with electronic transition of ZnO/ZnNb2O6/Nb2O5 composite, Ceram. Int. 47 (2021) 24732–24742, https://doi.org/10.1016/j.ceramint.2021.05.196.
[20] G. Essalah, H. Guermazi, S. Guermazi, G. Leroy, B. Duponchel, M. Mascot, C. Poupin, A. Rao, S. Mangavati, Enhanced dielectric properties of ternary ZnO-based composites for dielectric applications, Appl. Phys. A 128 (2022) 1–12, https://doi.org/10.1007/s00339-021-05123-2.
[21] G. Ren, D. Hu, E.W.C. Cheng, M.A. Vargas-Reus, P. Reip, R.P. Allaker, Characterisation of copper oxide nanoparticles for antimicrobial applications, Int. J. Antimicrob. Agents 33 (2009) 587–590, https://doi.org/10.1016/j.ijantimicag.2008.12.004.
[22] S.-M. Lam, J.-C. Sin, I. Satoshi, A.Z. Abdullah, A.R. Mohamed, Enhanced sunlight photocatalytic performance over Nb2O5/ZnO nanorod composites and the mechanism study, Appl. Catal. Gen. 471 (2014) 126–135, https://doi.org/10.1016/j.apcata.2013.12.001.
[23] J. Arul Mary, J. Judith Vijaya, M. Bououdina, L. John Kennedy, J.H. Daie, Y. Song, Investigation of structural, surface morphological, optical properties and first-principles study on electronic and magnetic properties of (Ce, Fe)-co doped ZnO, Phys. B Condens. Matter 456 (2015) 344–354, https://doi.org/10.1016/j.physb.2014.09.023.
[24] S. Fabbiyola, V. Sailaja, L.J. Kennedy, M. Bououdina, J. Judith Vijaya, Optical and magnetic properties of Ni-doped ZnO nanoparticles, J. Alloys Compd. 694 (2017) 522–531, https://doi.org/10.1016/j.jallcom.2016.10.022.
[25] W. Lopes de Almeida, N.S. Ferreira, F.S. Rodembusch, V. Caldas de Sousa, Study of structural and optical properties of ZnO nanoparticles synthesized by an eco-friendly tapioca-assisted route, Mater. Chem. Phys. 258 (2021), 123926, https://doi.org/10.1016/j.matchemphys.2020.123926.
[26] S.K. Noukelag, H.E.A. Mohamed, B. Moussa, L.C. Razanamahandry, S.K. O. Ntwampe, C.J. Arendse, M. Maaza, Investigation of structural and optical properties of biosynthesized Zincite (ZnO) nanoparticles (NPs) via an aqueous extract of Rosmarinus officinalis (rosemary) leaves, MRS Adv 5 (2020) 2349–2358, https://doi.org/10.1557/adv.2020.220.
[27] A.A. Atta, M.M. El-Nahass, A.M. Hassanien, K.M. Elsabawy, M.M. Abd El-Raheem, A. Alhuthali, S.E. Alomariy, M.S. Algamdi, Effect of thermal annealing on structural, optical and electrical properties of transparent Nb2O5 thin films, Mater. Today Commun. 13 (2017) 112–118, https://doi.org/10.1016/j.mtcomm.2017.09.004.
[28] T.B. Atisme, C.-Y. Yu, E.N. Tseng, Y.-C. Chen, P.-K. Hsu, S.-Y. Chen, Interface interactions in conjugated polymer composite with metal oxide nanoparticles, Nanomaterials 9 (2019), https://doi.org/10.3390/nano9111534.
[29] Q.M. Al-Bataineh, AhmadA. Ahmad, A.M. Alsaad, A.D. Telfah, Optical characterizations of PMMA/metal oxide nanoparticles thin films: bandgap engineering using a novel derived model, Heliyon 7 (2021), e05952, https://doi.org/10.1016/j.heliyon.2021.e05952.
[30] R.A. Rani, F.N. Omar, M.H. Fadzilah Suhaimi, A.S. Zoolfakar, M.H. Mamat, S. Alrokayan, H.A. Khan, M.R. Mahmood, Engineering the properties of Nb2O5-ZnO nanostructures via dual synthesis techniques, in: 2018 IEEE Int. Conf. Semicond. Electron. ICSE, IEEE, Kuala Lumpur, 2018, pp. 1–4, https://doi.org/10.1109/SMELEC.2018.8481206.
[31] C. Mrabet, O. Kamoun, A. Boukhachem, M. Amlouk, T. Manoubi, Some physical investigations on hexagonal-shaped nanorods of lanthanum-doped ZnO, J. Alloys Compd. 648 (2015) 826–837, https://doi.org/10.1016/j.jallcom.2015.07.009.
[32] R. Zamiri, A.F. Lemos, A. Reblo, H.A. Ahangar, J.M.F. Ferreira, Effects of rare-earth (Er, La and Yb) doping on morphology and structure properties of ZnO nanostructures prepared by wet chemical method, Ceram. Int. 1 (2014) 523–529, https://doi.org/10.1016/j.ceramint.2013.06.034.
[33] R. Boughalmi, A. Boukhachem, I. Gaied, K. Boubaker, M. Bouhafs, M. Amlouk, Effect of tin content on the electrical and optical properties of sprayed silver sulfide semiconductor thin films, Mater. Sci. Semicond. Process. 16 (2013) 1584–1591, https://doi.org/10.1016/j.mssp.2013.05.019.
[34] C. Aydın, M.S. Abd El-sadek, K. Zheng, I.S. Yahia, F. Yakuphanoglu, Synthesis, diffused reflectance and electrical properties of nanocrystalline Fe-doped ZnO via sol–gel calcination technique, Opt Laser. Technol. 48 (2013) 447–452, https://doi.org/10.1016/j.optlastec.2012.11.004.
[35] J.I. Pankove, Optical Processes in Semiconductors, 1971.
[36] A. Lucarelli, S. Lupi, P. Calvani, P. Maselli, G. De Marzi, P. Roy, N.L. Saini, A. Bianconi, T. Ito, K. Oka, Optical conductivity of the nonsuperconducting cuprate ${\mathrm{La}}_{8\ensuremath{-}x}{\mathrm{Sr}}_{x}{\mathrm{Cu}}_{8}{\mathrm{O}}_{20}$, Phys. Rev. B 65 (2002), 054511 https://doi.org/10.1103/PhysRevB.65.054511.
[37] V. Ganesh, L. Haritha, H.E. Ali, A.M. Aboraia, Y. Khairy, H.H. Hegazy, V. Butova, A.V. Soldatov, H. Algarni, H.Y. Zahran, I.S. Yahia, The detailed calculations of optical properties of indium-doped CdO nanostructured films using Kramers-Kronig relations, J. Non-Cryst. Solids 552 (2021), 120454, https://doi.org/10.1016/j.jnoncrysol.2020.120454.
[38] P.M. Dinakaran, S. Kalainathan, Studies on the optical and mechanical properties of organic nonlinear optical 1-(4-fluorostyryl)-4-nitrostilbene (FNS) single crystal, Optik 124 (2013) 5111–5115, https://doi.org/10.1016/j.ijleo.2013.03.073.
[39] H.S. Bolarinwa, M.U. Onuu, A.Y. Fasasi, S.O. Alayande, L.O. Animasahun, I. O. Abdulsalami, O.G. Fadodun, I.A. Egunjobi, Determination of optical parameters of zinc oxide nanofibre deposited by electrospinning technique, J. Taibah Univ. Sci. 11 (2017) 1245–1258, https://doi.org/10.1016/j.jtusci.2017.01.004.
[40] C. Abed, S. Fernández, H. Elhouichet, Studies of optical properties of ZnO:MgO thin films fabricated by sputtering from home-made stable oversize targets, Optik 216 (2020), 164934, https://doi.org/10.1016/j.ijleo.2020.164934.
[41] A. Douayar, M. Abd-Lefdil, K. Nouneh, P. Prieto, R. Diaz, A.O. Fedorchuk, I. V. Kityk, Photoinduced Pockels effect in the Nd-doped ZnO oriented nanofilms, Appl. Phys. B 110 (2013) 419–423, https://doi.org/10.1007/s00340-012-5271-7.
[42] I.V. Kityk, N.S. AlZayed, K. Kobayashi, X. Chen, M. Oyama, A.M. El-Naggar, A. A. Albassam, Influence of Al-doped ZnO and Ga-doped ZnO substrates on third harmonic generation of gold nanoparticles, Phys. E Low-Dimens. Syst. Nanostructures. 71 (2015) 91–95, https://doi.org/10.1016/j.physe.2015.04.003.
[43] E.M. Rockafellow, L.K. Stewart, W.S. Jenks, Is sulfur-doped TiO2 an effective visible light photocatalyst for remediation? Appl. Catal. B Environ. 91 (2009) 554–562, https://doi.org/10.1016/j.apcatb.2009.06.027.
[44] I. Daou, O. Zegaoui, A. Elghazouani, Physicochemical and photocatalytic properties of the ZnO particles synthesized by two different methods using three different precursors, Compt. Rendus Chem. 20 (2017) 47–54, https://doi.org/10.1016/j.crci.2016.04.003.
[45] J. Sin, Y. Chin, S.-M. Lam, WO3/Nb2O5 nanoparticles-decorated hierarchical porous ZnO microspheres for enhanced photocatalytic degradation of palm oil mill effluent and simultaneous production of biogas, Key Eng. Mater. 821 (2019) 379–385. https://doi.org/10.4028/www.scientific.net/KEM.821.379.
[46] V.-P. Dinh, T.-D.-T. Huynh, H.M. Le, V.-D. Nguyen, V.-A. Dao, N.Q. Hung, L. A. Tuyen, S. Lee, J. Yi, T.D. Nguyen, L.V. Tan, Insight into the adsorption mechanisms of methylene blue and chromium(III) from aqueous solution onto pomelo fruit peel, RSC Adv. 9 (2019) 25847–25860, https://doi.org/10.1039/C9RA04296B.
[47] M.J. Haque, M.M. Bellah, M.R. Hassan, S. Rahman, Synthesis of ZnO nanoparticles by two different methods &amp$\mathsemicolon$ comparison of their structural, antibacterial, photocatalytic and optical properties, Nano Express 1 (2020), 010007, https://doi.org/10.1088/2632-959X/ab7a43.
[48] G. Pereira Costa, R.A. Rafael, J.C.S. Soares, A.B. Gaspar, Synthesis and characterization of ZnO-Nb2O5 catalysts for photodegradation of bromophenol blue, Catal. Today 344 (2020) 240–246, https://doi.org/10.1016/j.cattod.2019.04.059.
[49] L. Wang, Y. Li, P. Han, Y. Jiang, Facile fabrication of Fe-doped Nb2O5 nanofibers by an electrospinning process and their application in photocatalysis, RSC Adv. 11 (2020) 462–469, https://doi.org/10.1039/D0RA10042K.
[50] J.P. Shubha, S.F. Adil, M. Khan, M.R. Hatshan, A. Khan, Facile fabrication of a ZnO/Eu2O3/NiO-based ternary heterostructure nanophotocatalyst and its application for the degradation of methylene blue, ACS Omega 6 (2021) 3866–3874, https://doi.org/10.1021/acsomega.0c05670.
[51] N. Raghavan, S. Thangavel, G. Venugopal, Enhanced photocatalytic degradation of methylene blue by reduced graphene-oxide/titanium dioxide/zinc oxide ternary nanocomposites, Mater. Sci. Semicond. Process. 30 (2015) 321–329, https://doi.org/10.1016/j.mssp.2014.09.019.
[52] K.A. Isai, V.S. Shrivastava, Photocatalytic degradation of methylene blue using ZnO and 2%Fe–ZnO semiconductor nanomaterials synthesized by sol–gel method: a comparative study, SN Appl. Sci. 1 (2019) 1247, https://doi.org/10.1007/s42452-019-1279-5.
[53] Y. Yuniar, T. Mawarni, P.L. Hariani, M. Faizal, T.E. Agustina, Degradation of Methylene Blue Dye Using ZnO/$NiFe_2O_4$ Photocatalyst under Visible Light, Atlantis Press, 2022, pp. 90–95, https://doi.org/10.2991/ahe.k.220205.016.
[54] L.P.P. Ha, T.H.T. Vinh, N.T.B. Thuy, C.M. Thi, P.V. Viet, Visible-light-driven photocatalysis of anisotropic silver nanoparticles decorated on ZnO nanorods:

synthesis and characterizations, J. Environ. Chem. Eng. 9 (2021), 105103, https://doi.org/10.1016/j.jece.2021.105103.
[55] T. Aloui, H. Guermazi, N. Fourati, C. Zerrouki, S. Guermazi, Synthesis and characterization of nanosheet NiMoO4 powder as a highly efficient and reusable catalyst for environmental remediation, J. Nanoparticle Res. 24 (2022) 1–15, https://doi.org/10.1007/s11051-022-05417-3.
[56] A. Kogo, Y. Numata, M. Ikegami, T. Miyasaka, Nb2O5 blocking layer for high open-circuit voltage perovskite solar cells, Chem. Lett. 44 (2015) 829–830, https://doi.org/10.1246/cl.150167.